

Frequency-independent voltage amplitude across a tunnel junction

Simon Feigl,^{1, a)} Radovan Vranik,¹ Bareld Wit,¹ and Stefan Müllegger^{1,2}

¹⁾*Institute of Semiconductor and Solid State Physics, Johannes Kepler University Linz, 4040 Linz, Austria.*

²⁾*Linz Institute of Technology, Johannes Kepler University Linz, 4040 Linz, Austria.*

(Dated: 28 October 2020)

Radio-frequency (rf) scanning tunneling microscopy has recently been advanced to methods like single-atom spin resonance. Such methods require a frequency-independent rf voltage amplitude across the tunnel junction, which opposes the strong frequency dependence of the rf attenuation in a transmission line. A reliable calibration of the voltage amplitude across the tunnel junction is therefore crucial. Two calibration methods have been reported to date, both compensating for the frequency dependent rf attenuation (transfer function), which first has to be determined. In this work we present a method to achieve a frequency-independent rf voltage amplitude across the tunnel junction that avoids the detour of determining the transfer function, thus reducing the complexity of the calibration. We applied the method on our rf scanning tunneling microscope and show the results of the manual calibration. We also show the transfer function of our rf transmission line up to 5.6 GHz. Although this work has been conducted with a rf scanning tunneling microscope, the presented procedures should also apply to any other device that can deliver rf voltage to a tunnel junction.

I. INTRODUCTION

Scanning tunneling microscopy (STM) methods have been in constant development since its invention around 40 years ago.^{1,2} One recently added method is radio-frequency scanning tunneling spectroscopy: voltage changes with radio-frequency (rf) are applied across the STM tunnel junction while the differential tunneling conductance (dI/dV) is recorded.³ With this technique we have demonstrated excitation of electron and nuclear spin transitions in single molecules,^{4,5} and have revealed mechanical eigenmodes of molecular resonators.⁶ A similar approach, well known as ESR-STM,^{7–12} is based on single-spin magnetoresistance detection and has recently enabled measurement of single-atom spin resonance.

One remaining technological challenge hampering the further development of rf STM is posed by the pronounced frequency dependence of the rf voltage amplitude across the tunnel junction ($V_{\text{pk, jun}}$). A variable $V_{\text{pk, jun}}$ may result in spurious measurement signals, which can easily be misinterpreted.^{13,14} Therefore, a method to achieve constant $V_{\text{pk, jun}}$ independent of frequency, is imperative. Currently no method exists to measure $V_{\text{pk, jun}}$ directly.¹¹ Two approaches for the determination of $V_{\text{pk, jun}}$ and its calibration to a constant value have been reported to date.^{13,14} They rely on the comparison of differential tunneling conductance spectra and on the frequency dependent rf voltage attenuation (transfer function, see Appendix C) obtained using a linearization method for the nonlinear current-voltage characteristic of the tunnel junction. In this work, we present a method to achieve a constant $V_{\text{pk, jun}}$ independent of the comparison of conductance spectra, transfer function and linearization, which is based on a recursive

algorithm.

II. RADIO-FREQUENCY SCANNING TUNNELING MICROSCOPE

We have conducted the experiments with a modified Createc low-temperature STM in ultra-high vacuum (UHV) conditions. The sample temperature is typically 8 K and the pressure below 5×10^{-11} mbar. We have upgraded the STM with rf-rated components, similar to our previously reported setup.^{4,6,15} The schematic of the electronics is shown in Figure 1 and all components are listed in Appendix A. This setup enables rapid modulation of the voltage across the tunnel junction at high frequencies, achieving a bandwidth of up to 5.6 GHz. The total voltage V_{tot} is composed of two components, V_{dc} and V_{rf} , which are superimposed:

$$V_{\text{tot}}(t) = V_{\text{dc}}(t) + V_{\text{rf}}(t). \quad (1)$$

Here t is time, V_{dc} is the slowly time-varying component (\leq few kHz) and V_{rf} is the fast time-varying component (rf voltage, MHz–GHz) with an amplitude of up to ≈ 100 mV, limited by the attenuation in the transmission line (see Appendix C).

It is convenient to consider the electronic setup as three parts as shown in Figure 1. The dc and rf parts cover the electronics and cabling associated purely with the STM control and frequency modulation, respectively. In the mixed part, from the bias tees onward, the signals are transmitted through the same cables. Note that rf voltage is transmitted via cryo dc cables, which have an insertion loss (see Appendix C) of more than 60 dB/m at 2 GHz. Their length is ≈ 15 cm each. Typical values of the insertion loss of all cables are given in Table II in Appendix A.

Although the insertion loss of the commercial electrical components is well specified, the determination of the to-

^{a)}simon.feigl@jku.at

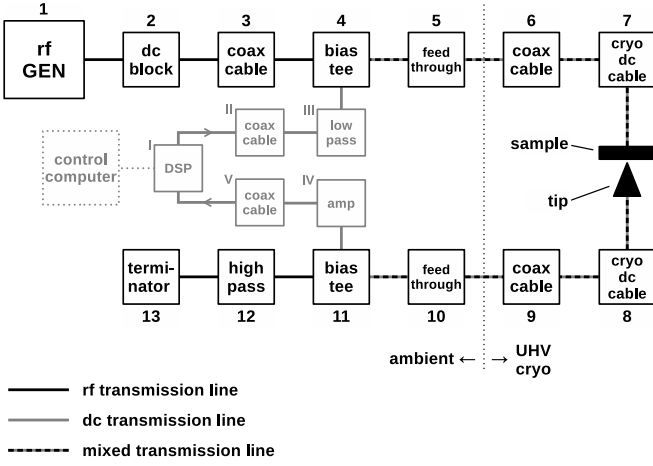


FIG. 1. Schematic of the electronic setup of our rf STM, highlighting the different components of the rf, dc and mixed transmission lines. The control computer as well as the region of cryogenic UHV conditions are indicated with dotted lines. Details of the numbered items are given in Table I in Appendix A.

tal insertion loss of the whole transmission line from the signal generator to the tunnel junction is not straightforward due to the complicated rf characteristics of the last few centimeters of the line, including the sample holder and sample.¹¹ A practical measurement of the total insertion loss is based on determining $V_{\text{pk,jun}}$.^{11,13,14,16} In Appendix B we describe our procedure for the determination of $V_{\text{pk,jun}}$, which is also suitable for other rf STM setups.

III. METHOD FOR ACHIEVING CONSTANT RF VOLTAGE AMPLITUDE ACROSS THE TUNNEL JUNCTION

If the power at the rf signal generator output (P_{gen}) is held constant, $V_{\text{pk,jun}}$ varies with changing frequency. Therefore, it is necessary to adjust P_{gen} to achieve a constant, frequency-independent $V_{\text{pk,jun}}$. We call this adjustment calibration of $V_{\text{pk,jun}}$.

For the calibration method, we make use of the rectification effect of the nonlinearity (step) in the dI/dV -spectrum of Ag(111). As explained in Appendix B, rectification of the tunneling current causes a broadening of the step in the dI/dV -spectrum, if a rf voltage is applied. Consequently, in the vicinity of the nonlinearity, the magnitude of the differential tunneling conductance depends on $V_{\text{pk,jun}}$. This dependence is illustrated in Figure 2 for a V_{dc} -value at the bottom of the step; the dI/dV -value increases with $V_{\text{pk,jun}}$ and thus with P_{gen} .

$V_{\text{pk,jun}}$ is frequency-independent, if the dI/dV -value measured at a fixed V_{dc} close to the nonlinearity is the same for each frequency. For Ag(111), a V_{dc} of -85 mV is chosen, because it is near the lower edge of the step, see Figure 2. For each frequency, P_{gen} is adjusted until the

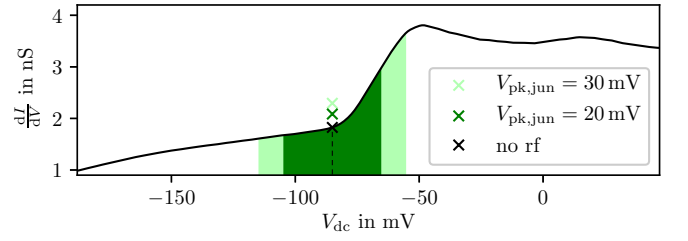


FIG. 2. dI/dV -spectrum of Ag(111) and the shift of one dI/dV -value when rf voltage is applied. The solid black curve is the average of 125 single dI/dV -spectra. The value of the dI/dV -spectrum at $V_{\text{dc}} = -85$ mV is marked with a black cross. When rf voltage is applied, the measured dI/dV -value increases due to rectification as explained in the text. The dark green cross marks the value when the rf voltage amplitude is 20 mV and the light green cross when it is 30 mV. The shaded areas of the same colors illustrate the intervals that influence the corresponding dI/dV -value at $V_{\text{dc}} = -85$ mV when rf voltage is applied.

dI/dV -value reaches a predefined target, see Figure 3. In order to obtain this target, the desired $V_{\text{pk,jun}}$ is chosen and the procedure described in Appendix B is used to find the power generator output to achieve this $V_{\text{pk,jun}}$ at a single frequency. The dI/dV -value at $V_{\text{dc}} = -85$ mV for that output power and frequency is then taken as the target value.

One advantage of this method is that it is not necessary to know the exact functional relation between P_{gen} and the dI/dV -value. In particular, the relation does not need to be linearized nor fitted, unlike in the previously reported methods.^{14,16} A restriction is that the relation has to be bijective in the region of interest. This can be verified by recording dI/dV at a fixed V_{dc} while sweeping P_{gen} . The nonlinearity causing the rectification has to be independent of the frequency and independent of the power of the rf voltage.

The success of the calibration can be quantified by determining the calibrated $V_{\text{pk,jun}}$ at each frequency and comparing it to the desired value. Figure 4 shows the result of a manual calibration. The desired value of 30 mV is met by the calibrated rf voltage amplitudes, which have a mean value of (30 ± 2) mV. With future automation we expect to reduce the variance of the calibrated amplitudes. Additionally, improvements of the cabling and instrumentation will decrease the measurement error and raise the upper bandwidth limit to higher frequencies. The calibration for each frequency value takes about two minutes and the measurement of $V_{\text{pk,jun}}$ about ten minutes, including analysis and documentation. Once the automation is implemented, we expect both procedures to become significantly faster.

Based on our method to determine $V_{\text{pk,jun}}$, we also derived the transfer function of our setup as detailed in Appendix C.

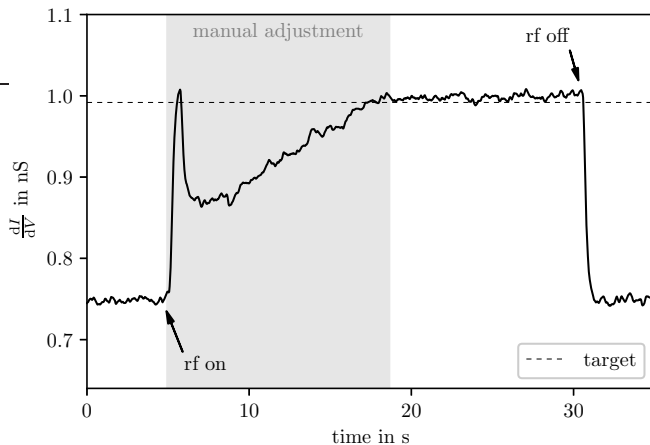


FIG. 3. Exemplary time evolution of the dI/dV -value at constant V_{dc} during calibration. In the first and last ≈ 4 s, no rf voltage was applied. The times when the rf signal generator was switched on and off are marked with the annotations *rf on* and *rf off*, respectively. After the rf signal generator was switched on, P_{gen} was adjusted until the target value was reached. The adjustment period is marked as *manual adjustment* and shaded in gray. The target dI/dV -value is drawn as a horizontal line. This example also highlights some potential issues with the manual procedure. Namely, the peak at ≈ 6 s is caused by an unintentional fast variation of P_{gen} . The slower increase after ≈ 7 s reflects the typical pace. Also, it is clear that some inaccuracy in the determination of the target value remains as the dI/dV value between ≈ 20 s and ≈ 30 s is slightly too high. Automation of the procedure will improve this.

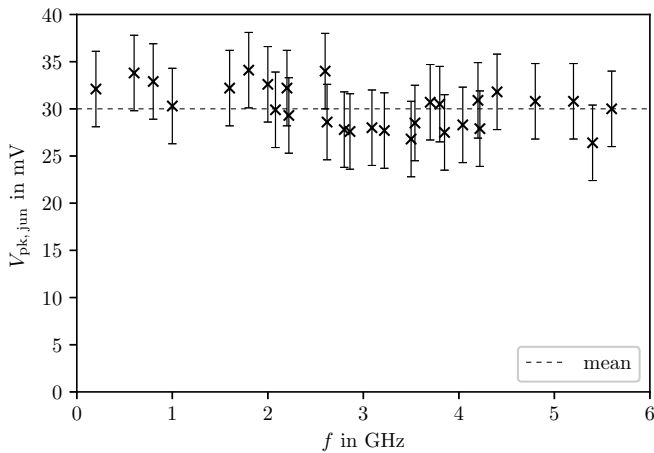


FIG. 4. Radio-frequency voltage amplitudes for 29 frequency values up to 5.6 GHz after manual calibration to the target value of 30 mV. The mean value of the calibrated amplitudes is (30 ± 2) mV, depicted by the dashed line. The frequency values were chosen by relevance to another experiment and are therefore not evenly distributed. With the future automation of the calibration we intend to reduce the variance of the amplitudes. Improvements of the cabling and instrumentation will reduce the measurement error and raise the upper bandwidth limit to higher frequencies.

IV. SUMMARY

Radio-frequency scanning tunneling spectroscopy is a powerful tool enabling, e.g., single-atom spin resonance. It requires a frequency-independent rf voltage amplitude across the tunnel junction, which is nontrivial. We have developed a new method to calibrate the rf voltage amplitude to a frequency-independent value. Unlike previously reported procedures, this method does not require the measurement of the transfer function of the rf transmission line, nor the linearization of the nonlinear current-voltage characteristic of the tunnel junction. First results show the successful application of our method: after calibration to the target value of 30 mV we measure a mean rf peak voltage across the tunnel junction of (30 ± 2) mV at 29 different frequencies up to 5.6 GHz. We also obtained the transfer function of the rf transmission line at these frequencies. Although this work has been achieved with a rf STM, we expect the described procedures to also apply to any other device that can deliver rf voltage to a tunnel junction.

V. ACKNOWLEDGEMENTS

This project has received funding from the European Research Council (ERC) under the European Union's Horizon 2020 research and innovation programme (grant agreement No 771193). The authors acknowledge the financial support of the Government of the Province of Upper Austria together with the Johannes Kepler University Linz (LIT project 2016-1-ADV-002).

VI. DATA AVAILABILITY STATEMENT

The data that support the findings of this study are available from the corresponding author upon reasonable request.

Appendix A: Details of the electronic components

Tables I and II show details of the electronic components of the setup described in the main text in Section II.

TABLE I. Electronic components used in the STM transmission lines. The first two columns (nr, name) refer to Figure 1. The characteristic line impedance of components 1–6 and 9–13 is $50\ \Omega$.

nr	name	description
rf and mixed transmission line		
1	rf GEN	rf signal generator, Keysight N5173B
2	dc block	Keysight N9398F
3	coax cable	Mini-Circuits CBL-12FT-SMSM+ (12 ft)
4	bias tee	Tektronix PSPL5541A
5	feedthrough	SMA on an UHV DN 16 CF flange
6	coax cable	Lake Shore cryogenic cable SR (1.5 m)
7	cryo dc cable	flexible cryogenic dc cable, < 0.15 m
8	cryo dc cable	flexible cryogenic dc cable, < 0.15 m
9	coax cable	Lake Shore cryogenic cable SR (1.5 m)
10	feedthrough	SMA on an UHV DN 16 CF flange
11	bias tee	Tektronix PSPL5541A
12	high pass	high pass filter, Mini-Circuits SHP-300+
13	terminator	Mini-Circuits, $50\ \Omega$
dc transmission line		
I	DSP	STM electronic control box, Createc 6711 DSP (digital signal processor)
II	coax cable	bedea RG58 (5 m)
III	low pass	low pass filter, Mini-Circuits BLP-1.9+
IV	amp	low noise current amplifier FEMTO DLPCA-200
V	coax cable	low noise cable FEMTO CAB-LN1-BB (3 m)

TABLE II. Typical values of the insertion loss of the cables used in the rf transmission line. The numbers and names correspond to those in Table I and Figure 1. N/A means no data available for this entry.

		frequency (GHz)						
		0.50	0.73	1.00	1.37	2.00	5.00	6.00
nr	name	insertion loss (dB/m)						
3	coax cable	N/A	0.33	N/A	0.45	0.56	N/A	1.04
6 & 9	coax cable	4.43	N/A	6.27	N/A	N/A	14.09	N/A
7 & 8	cryo dc cable	22.3	30.6	37.9	43.0	62.6	112.6	155.2

Appendix B: Determination of the rf voltage amplitude across the tunnel junction

The differential tunneling conductance (dI/dV) as a function of V_{dc} is measured with a lock-in amplifier. Typical values for the modulation rms voltage and frequency are a few mV and 773 Hz, respectively. We superimpose V_{rf} with frequencies up to several GHz. The resulting changes in dI/dV are too fast to be resolved by the lock-in amplifier, which outputs the time average of these changes.

If the time dependence of V_{rf} is known, a weight function (u) for this averaging process can be calculated; the probability of V_{rf} having a value in the interval $[V_{rf}, V_{rf} + dV_{rf}]$ is $u(V_{rf}) dV_{rf}$. This probability is also equal to the time spent in this interval (dt) divided by the total time, $1/(2f)$, that V_{rf} needs to run over all values between its extrema $-V_{pk,jun}$ and $+V_{pk,jun}$ once.¹⁷

$$u(V_{rf}) dV_{rf} = \frac{dt}{1/(2f)}. \quad (B1)$$

In our case, we use a sinusoidal modulation:

$$V_{rf}(t) = V_{pk,jun} \sin(2\pi ft) \quad (B2)$$

where $V_{pk,jun}$ is the peak voltage amplitude across the junction and f the frequency. Thus, differentiating Equation B2 and using the relation $\cos(2\pi ft) = \sqrt{1 - \sin^2(2\pi ft)}$, Equation B1 can be rewritten to give $u(V_{rf})$ explicitly,

$$u(V_{rf}) = \frac{1}{\pi V_{pk,jun} \sqrt{1 - \left(\frac{V_{rf}}{V_{pk,jun}}\right)^2}}. \quad (B3)$$

The weight function $u(V_{rf})$ has the shape of the probability density function of the arcsine distribution,¹⁸ see green line in Figure 5.

The time average of the differential tunneling conductance is obtained by convolution with $u(V_{rf})$,

$$\frac{dI}{dV}(V_{dc})|_{rf\ on} = \int_{-V_{pk,jun}}^{+V_{pk,jun}} \frac{dI}{dV}(V_{dc} + V_{rf})|_{rf\ off} u(V_{rf}) dV_{rf}, \quad (B4)$$

where $dI/dV|_{rf\ on}$ and $dI/dV|_{rf\ off}$ are the differential tunneling conductances with and without rf voltage applied, respectively. Figure 5 illustrates the convolution: the dI/dV -spectrum is averaged by the quickly oscillating V_{rf} . The sinusoidal V_{rf} leads to a symmetric weight function. Therefore, the averaging affects the dI/dV -value only when the dI/dV -spectrum is nonlinear in the averaging range,¹⁹ which is the V_{dc} -interval $[V_{dc} - V_{pk,jun}, V_{dc} + V_{pk,jun}]$. This well known effect of rectification at a nonlinearity has been described earlier in References 13, 14, 20–23.

In this work, we determine $V_{\text{pk, jun}}$ using the characteristic step in the dI/dV -spectrum of Ag(111) as non-linearity. Similar procedures have been successfully applied to spectroscopic features of, e.g., a Co atom on MgO/Ag(001).¹⁴ The step corresponds to the onset of the electronic surface state near -70 mV.²⁴ When measured with V_{rf} applied, this step is broadened, as shown in Figure 5. Based on Equation B4 we determine $V_{\text{pk, jun}}$ by a series of dI/dV -measurements and a computer simulation. We record the dI/dV -spectrum of Ag(111) without V_{rf} and the dI/dV -spectrum with V_{rf} switched on (the latter is herein denoted by *rf dI/dV -spectrum*). The dI/dV -spectra are averages of five consecutive measurements at the same location on the silver surface. They are recorded typically within one minute to minimize the effects of slow changes at the tunnel junction such as thermal drift or a tip apex rearrangement.

Since $u(V_{\text{rf}})$ is a function of $V_{\text{pk, jun}}$, see Equation B3, $V_{\text{pk, jun}}$ can be used as an independent variable (simulation parameter) in the computer simulation. For a set of test values of $V_{\text{pk, jun}}$ the dI/dV -spectrum without V_{rf} is convolved with $u(V_{\text{rf}})$, yielding simulated *rf dI/dV -spectra*. These, we compare to the measured *rf dI/dV -spectrum* by a least-squares analysis. The simulated spectrum with the lowest sum of squared residuals yields our best guess for the value of $V_{\text{pk, jun}}$. An additional analysis of the residuals is used to identify unreliable simulation results due to the aforementioned slow changes at the tunnel junction that can occur during measurements. An example of the dI/dV -spectra used for the determination of $V_{\text{pk, jun}}$ at one single frequency is shown in Figure 5. The simulated *rf dI/dV -spectrum* agrees very well with the measured *rf dI/dV -spectrum*.

Appendix C: Transfer function

The electric power loss between two points 1 and 2 along a *rf* transmission line is frequency-dependent.²⁵ We describe the power loss with the frequency-dependent transfer function T_{P} . It is defined by

$$T_{\text{P}} := 10 \log_{10} \left(\frac{P_2}{P_1} \right) \quad (\text{C1})$$

where P_1 and P_2 are the powers in watts at point 1 and point 2, respectively. The subscript P signifies that this definition is based on the ratio of powers. T_{P} is a level quantity,²⁵ i.e., it compares two values. The unit of T_{P} is the decibel (dB). Note that the insertion loss²⁵ of the transmission line between the points 1 and 2 is $-T_{\text{P}}$.

It is common to express the power (P) of a *rf* voltage signal compared to the fixed reference value of 1 mW. This defines the power level ($^{\text{dBm}}P$) as

$$^{\text{dBm}}P := 10 \log_{10} \left(\frac{P}{0.001} \right). \quad (\text{C2})$$

Its unit is the dBm. Note that $^{\text{dBm}}P$ is a level quantity and it is therefore intrinsically different from the power

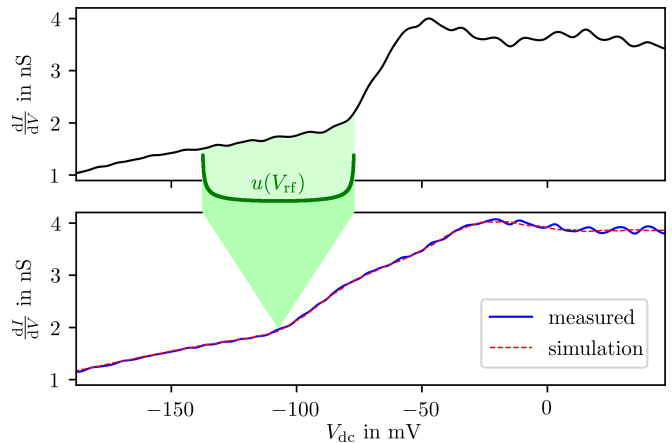


FIG. 5. Typical dI/dV -spectra of Ag(111) obtained with a tungsten tip. At the top, the dI/dV -spectrum without *rf* voltage applied is shown. The step around -70 mV corresponds to the onset of the electronic surface state. At the bottom, the measured and simulated dI/dV -spectra with *rf* voltage applied are shown. The broadening of the step as explained in the text is clearly visible. The corresponding weight function $u(V_{\text{rf}})$ (green line) and the averaging effect of V_{rf} (shaded green areas) are illustrated: The dI/dV -value of one single point in the dI/dV -spectrum with *rf* voltage applied is composed of all values of the dI/dV -spectrum without *rf* voltage applied that lie in the range $[V_{\text{dc}} - V_{\text{pk, jun}}, V_{\text{dc}} + V_{\text{pk, jun}}]$. Here, $V_{\text{pk, jun}}$ is 31 mV, so the range, equal to the width of $u(V_{\text{rf}})$, is 62 mV. The bottom plot also demonstrates the good agreement of the simulation with the measurement.

quantity P . Expressing P in terms of $^{\text{dBm}}P$, Equation C1 becomes

$$T_{\text{P}} = ^{\text{dBm}}P_2 - ^{\text{dBm}}P_1 \quad (\text{C3})$$

where $^{\text{dBm}}P_1$ and $^{\text{dBm}}P_2$ are the power levels at point 1 and point 2, respectively.²⁶

In order to characterize the whole transmission line, here the output of the *rf* signal generator is chosen as point 1 and the sample surface as point 2, giving

$$T_{\text{P}} = ^{\text{dBm}}P_{\text{sam}} - ^{\text{dBm}}P_{\text{gen}} \quad (\text{C4})$$

where $^{\text{dBm}}P_{\text{sam}}$ and $^{\text{dBm}}P_{\text{gen}}$ are the corresponding power levels.

In practice, it is convenient to express the transfer function in terms of a ratio of voltages rather than powers. The conversion from power to voltage requires knowledge about the impedance.²⁵ The mean power dissipated by an ohmic impedance (R) in a *rf* circuit is

$$P = \frac{V_{\text{rms}}^2}{R} \quad (\text{C5})$$

where V_{rms} is the root mean square voltage. For sinusoidal modulation, it is related to the peak voltage (V_{pk}) by

$$V_{\text{pk}} = V_{\text{rms}} \sqrt{2}. \quad (\text{C6})$$

The conversion between ${}^{\text{dBm}}P$ and V_{pk} can be done using Equations C2, C5 and C6, giving

$$V_{\text{pk}} = \sqrt{\frac{2R}{1000}} 10^{(\text{dBm}_P/10)}. \quad (\text{C7})$$

When using the line impedance of our components of 50Ω , Equation C7 simplifies to

$$V_{\text{pk}} = \sqrt{10^{(\frac{\text{dBm}_P}{10}-1)}}. \quad (\text{C8})$$

Equation C8 is valid for ${}^{\text{dBm}}P$ in dBm and V_{pk} in V.

Using Equation C5, Equation C1 can be transformed to

$$T_{\text{P}} = 20 \log_{10} \left(\frac{V_2}{V_1} \right) - 10 \log_{10} \left(\frac{R_2}{R_1} \right) \quad (\text{C9})$$

where V_1 and V_2 are the voltages at point 1 and point 2, respectively, and R_1 and R_2 the corresponding line impedances. V_1 and V_2 have to be the same entity, e.g., V_{rms} or V_{pk} . If the impedances are the same, the second term vanishes. Considering the abovementioned locations (point 1: output of the rf signal generator, point 2: sample surface), this may not be the case in general. Therefore we define a separate transfer function T , which is independent of the impedances (cf. Reference 16),

$$T := 20 \log_{10} \left(\frac{V_2}{V_1} \right). \quad (\text{C10})$$

Here, V_2 corresponds to $V_{\text{pk,jun}}$ and V_1 to the peak amplitude of the voltage of the rf signal generator output ($V_{\text{pk,gen}}$). Hence,

$$T := 20 \log_{10} \left(\frac{V_{\text{pk,jun}}}{V_{\text{pk,gen}}} \right). \quad (\text{C11})$$

With the measured rf voltage amplitudes across the tunnel junction, the corresponding P_{gen} and Equation C8, we calculated the transfer function T according to Equation C11. T as a function of the frequency is shown in Figure 6. Its value varies from (-3 ± 1) dB at 0.2 GHz to (-46 ± 1) dB at 5.4 GHz. Below 1 GHz, it stays above -20 dB. Between 1 and 5 GHz it varies between -20 and -40 dB. Between 5 and 6 GHz it drops below -40 dB.

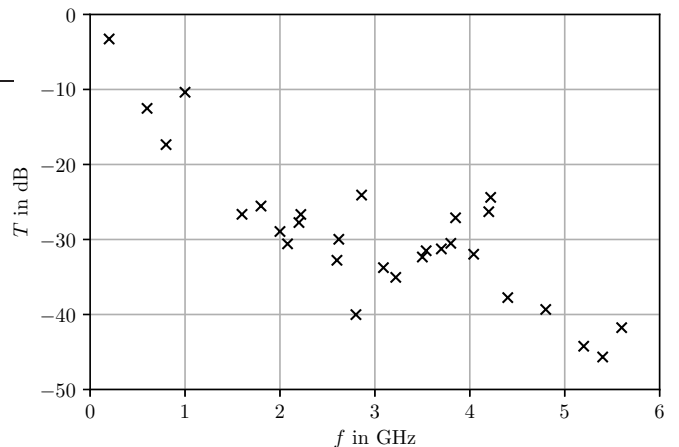


FIG. 6. Transfer function of our rf STM according to Equation C11, measured with a constant rf voltage amplitude of (30 ± 2) mV across the tunnel junction. The error of the data points is ± 1 dB.

- ⁶S. Müllegger, M. Rashidi, K. Mayr, M. Fattinger, A. Ney, and R. Koch, *Phys. Rev. Lett.* **112**, 117201 (2014).
- ⁷S. Baumann, W. Paul, T. Choi, C. P. Lutz, A. Ardavan, and A. J. Heinrich, *Science* **350**, 417 (2015).
- ⁸F. D. Natterer, K. Yang, W. Paul, P. Willke, T. Choi, T. Greber, A. J. Heinrich, and C. P. Lutz, *Nature* **543**, 226 (2017).
- ⁹T. Choi, C. Lutz, and A. Heinrich, *Curr. Appl. Phys.* **17**, 1513 (2017).
- ¹⁰P. Willke, W. Paul, F. D. Natterer, K. Yang, Y. Bae, T. Choi, J. Fernández-Rossier, A. J. Heinrich, and C. P. Lutz, *Sci. Adv.* **4** (2018).
- ¹¹F. D. Natterer, F. Patthey, T. Bilgeri, P. R. Forrester, N. Weiss, and H. Brune, *Rev. Sci. Instrum.* **90**, 013706 (2019).
- ¹²K. Yang, P. Willke, Y. Bae, A. Ferrón, J. L. Lado, A. Ardavan, J. Fernández-Rossier, A. J. Heinrich, and C. P. Lutz, *Nat. Nanotechnol.* **13**, 1120 (2018).
- ¹³M. Herve, M. Peter, and W. Wulfhekel, *Appl. Phys. Lett.* **107**, 093101 (2015).
- ¹⁴W. Paul, S. Baumann, C. P. Lutz, and A. J. Heinrich, *Rev. Sci. Instrum.* **87**, 074703 (2016).
- ¹⁵S. Müllegger, A. K. Das, K. Mayr, and R. Koch, *Nanotechnology* **25**, 135705 (2014).
- ¹⁶T. S. Seifert, S. Kovarik, C. Nistor, L. Persichetti, S. Stepanow, and P. Gambardella, *Phys. Rev. Research* **2**, 013032 (2020).
- ¹⁷Half a period is the time needed for V_{rf} to run from $-V_{\text{pk,jun}}$ to $+V_{\text{pk,jun}}$ *once*. It leads to the normalization of $\int_{-V_{\text{pk,jun}}}^{+V_{\text{pk,jun}}} u(V_{\text{rf}}) dV_{\text{rf}} = 1$. If, as one might think intuitively, the whole period is taken, then V_{rf} runs over each value *twice*, leading to a different normalization.
- ¹⁸Springer Verlag GmbH and European Mathematical Society, *Arcsine distribution* (accessed May 2020).
- ¹⁹For a detailed discussion of the suitable shape of the nonlinearity see Reference 20.
- ²⁰H. Q. Nguyen, P. H. Cutler, T. E. Feuchtwang, Z. . Huang, Y. Kuk, P. J. Silverman, A. A. Lucas, and T. E. Sullivan, *IEEE Trans. Electron Devices* **36**, 2671 (1989).
- ²¹W. Krieger, T. Suzuki, M. Völcker, and H. Walther, *Phys. Rev. B* **41**, 10229 (1990).
- ²²X. W. Tu, J. H. Lee, and W. Ho, *J. Chem. Phys.* **124**, 021105 (2006).
- ²³M. Völcker, W. Krieger, and H. Walther, *Phys. Rev. Lett.* **66**, 1717 (1991).
- ²⁴J. Li, W.-D. Schneider, R. Berndt, O. R. Bryant, and S. Crampin, *Phys. Rev. Lett.* **81**, 4464 (1998).

¹G. Binnig, H. Rohrer, C. Gerber, and E. Weibel, *Appl. Phys. Lett.* **40**, 178 (1982).

²G. Binnig, H. Rohrer, C. Gerber, and E. Weibel, *Phys. Rev. Lett.* **49**, 57 (1982).

³R. Koch and S. Müllegger, in *Molecular Architectonics*, edited by T. Ogawa (Springer International Publishing, Cham, 2017) pp. 187–218.

⁴S. Müllegger, S. Tebi, A. K. Das, W. Schöfberger, F. Faschinger, and R. Koch, *Phys. Rev. Lett.* **113**, 133001 (2014).

⁵S. Müllegger, E. Rauls, U. Gerstmann, S. Tebi, G. Serrano, S. Wiespointner-Baumgarthuber, W. G. Schmidt, and R. Koch, *Phys. Rev. B* **92**, 220418 (2015).

²⁵D. M. Pozar, *Microwave engineering* (Fourth edition. Hoboken, NJ : Wiley, 2012).

²⁶When subtracting two level quantities with the unit dBm, the result is a level quantity in dB. Substitution of Definition C2 into Equation C3 and a short calculation make this clear.